澳門大學
UNIVERSIDADE DE MACAU
UNIVERSITY OF MACAU

ROSIA: Rotation-Search-Based Star Identification Algorithm

Name:Xu Taosi

Email:XuTaosi@163.com

ROSIA: Rotation-Search-Based Star Identification Algorithm

Chee-Kheng Chng; Álvaro Parra Bustos; Benjamin McCarthy; Tat-Jun Chin

IEEE Transactions on Aerospace and Electronic Systems

Year: 2023 | Volume: 59, Issue: 5 | Journal Article |

Publisher: IEEE

Abstract HTML

What is the ROSIA

a rotation-search-based approach for addressing the star identification (Star-ID) problem, The proposed algorithm, ROSIA, is a heuristics-free algorithm that seeks the optimal rotation that maximally aligns the input and catalog stars in their respective coordinates.

Previous Star-ID algorithms

Subgraph-Isomorphism-Based Methods（子图同构）：

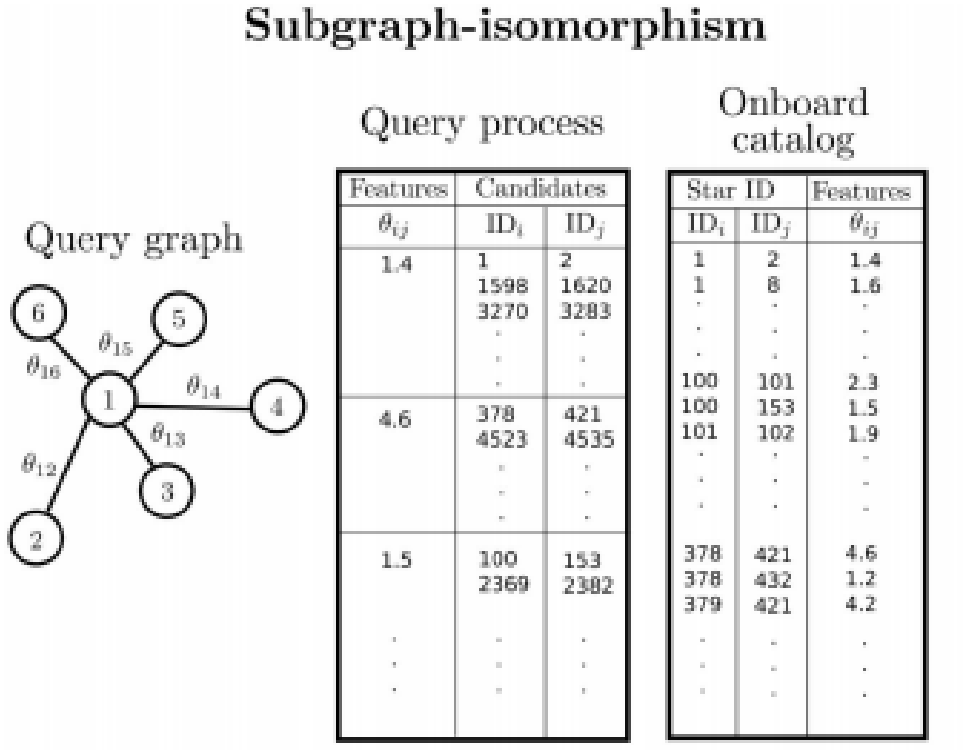

The subgraph isomorphism method typically employs a bottom-up approach for subgraph matching, and its drawback is the requirement for a large static memory to store the star catalog.

Previous Star-ID algorithms

Pattern-Recognition-Based Methods（模式识别法）：

The pattern-recognition-based methods (middle) first generate a query pattern with the input scene upon preprocessing heuristics, which rely on a subset of the stars (indicated by blue cells). Then, the query pattern is used to query the database, and the closest match is returned.

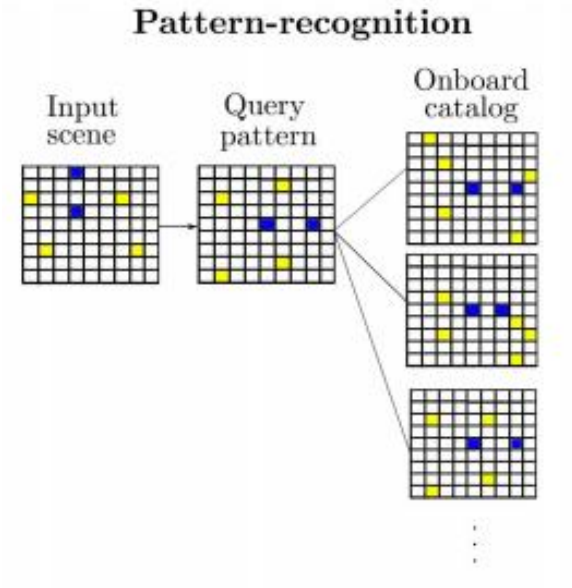

The derivations and effectiveness of the objective and upper bound functions of ROSIA

1. Wahba's Problem: Wahba's problem seeks to find the 3-D rotation that relates two reference frames from a set of corresponding vectors

$$\sum_{i=1}^{N} \|\mathbf{R}\mathbf{s}_i - \mathbf{c}_i\|$$

S_i : a detected star (unit) vector in the input star
C_i : its corresponding catalog star in the inertial frame

The derivations and effectiveness of the objective and upper bound functions of ROSIA

Wahba's problem is the goal of the attitude estimation module in a star tracker system

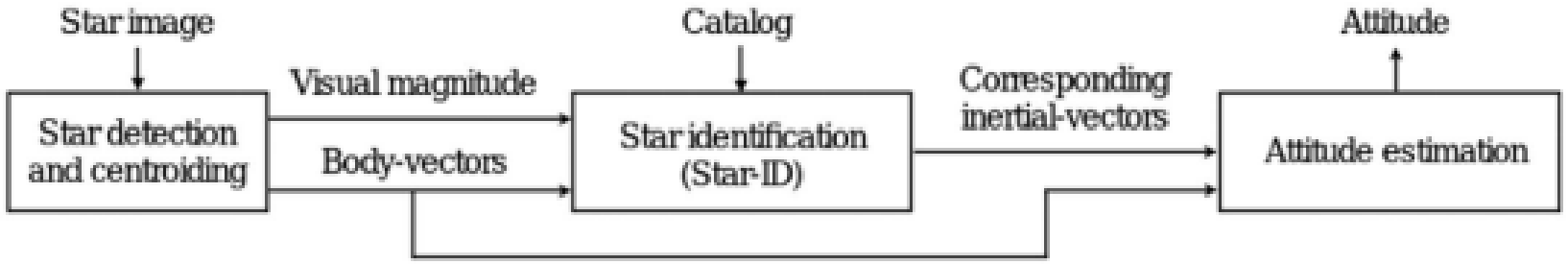

Fig. 1. Established attitude determination pipeline of a star tracker.

The derivations and effectiveness of the objective and upper bound functions of ROSIA

2. Correspondence-Free Rotation-Only Point Cloud Registration（无对应旋转点云配准）: is the general form of Wahba's problem, where the correspondences are unknown.

$$Q_{\text{euc}}(\mathbf{R}) = \sum_{i=1}^{N} \max_{1 \le j \le M} \lfloor \|\mathbf{R}\mathbf{s}_i - \mathbf{c}_j\| \le \epsilon \rfloor \qquad (2)$$

$Q_{euc}(R)$: This symbol represents the Euclidean distance metric.

$\lfloor\ \rfloor$:is an indicator function that returns 1 if the internal relation is true and 0.

The max operation : is in place to ensure one query star si only contributes at most one vote to the overall objective.

The derivations and effectiveness of the objective and upper bound functions of ROSIA

$$Q_{\text{ang}}(\mathbf{R}) = \sum_{i=1}^{N} \max_{1 \le j \le M} \lfloor \angle(\mathbf{R}\mathbf{s}_i,\ \mathbf{c}_j) \le \alpha_\epsilon \rfloor \qquad (3)$$

Qang(R): This symbol represents the angular distance metric.

Associating with the maximum Qang is also the largest catalog subset, where the identity of each detected stars can be expressed as

$M^* = \{\{i \boxed{\leftrightarrow} j\}_{i=1}^{N} | \sum_{i=1}^{N} max_{1 \le j \le M} \lfloor \angle(R^* S_i, C_j) \le \alpha_\epsilon \rfloor \ \forall i\}$

•M*: This represents the set M*, which stores the index pairs of point pairs that satisfy the conditions.

•{i $\boxed{\leftrightarrow}$ j}N: This represents the set of index pairs (i $\boxed{\leftrightarrow}$ j) of point pairs

the goal of this equation is to find the index pairs of point pairs that satisfy the conditions,.These index pairs can be used to represent the correspondence between detected matching point pairs during the registration process.

The derivations and effectiveness of the objective and upper bound functions of ROSIA

$$Q_{\text{ang}}(\mathbf{R}) = \sum_{i=1}^{N} \max_{1 \le j \le M} \lfloor \angle(\mathbf{R}\mathbf{s}_i,\ \mathbf{c}_j) \le \alpha_\epsilon \rfloor \qquad (3)$$

To solve (3) with BnB, we need an upper bound function to evaluate whether a subdomain in the rotation space should be further explored (branched).

BnB

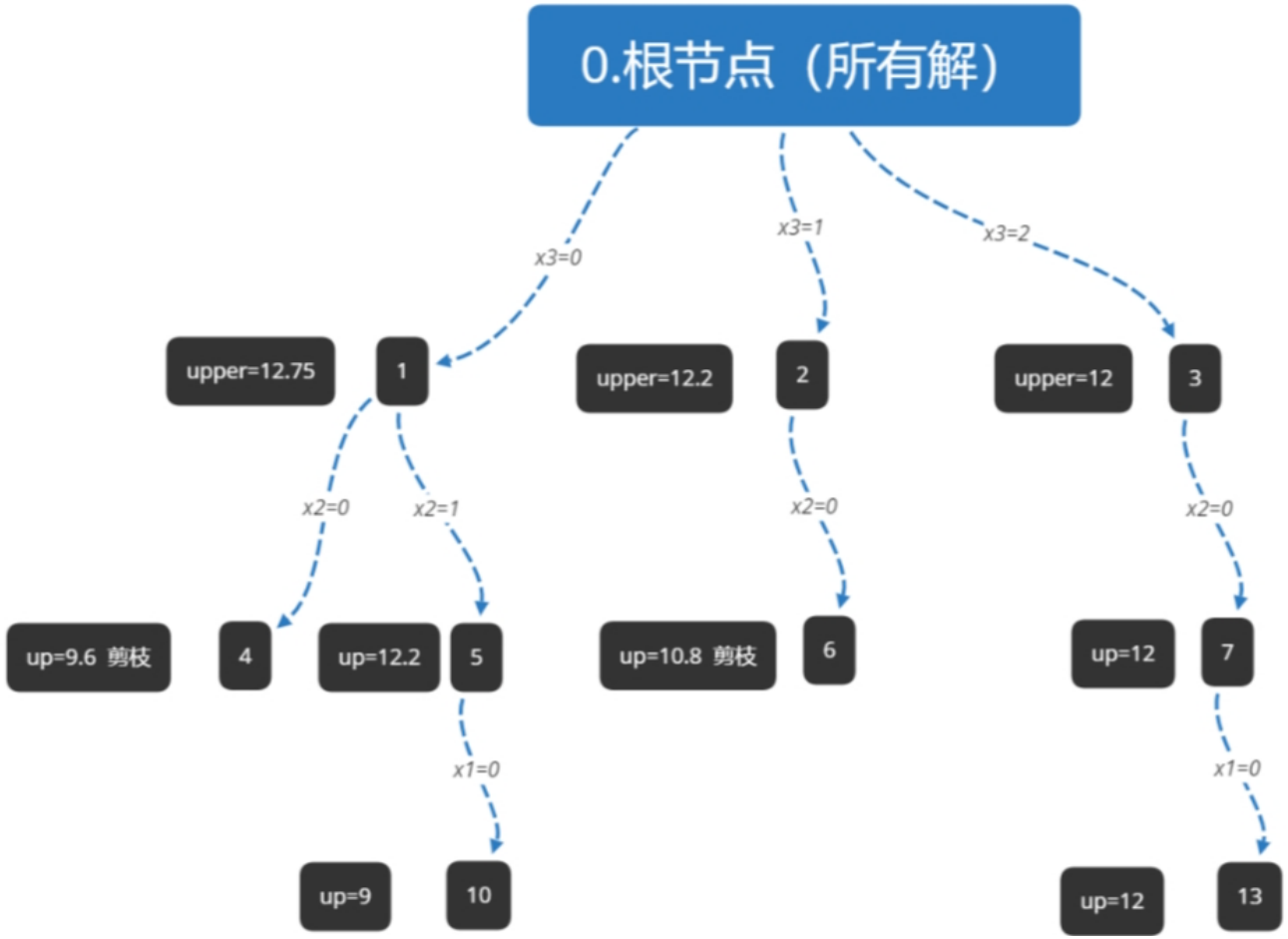
0.根节点（所有解）
x3=0
x3=1
x3=2
upper=12.75
1
upper=12.2
2
upper=12
3
x2=0
x2=1
x2=0
x2=0
up=9.6 剪枝
4
up=12.2
5
up=10.8 剪枝
6
up=12
7
x1=0
x1=0
up=9
10
up=12
13

The derivations and effectiveness of the objective and upper bound functions of ROSIA

3. Rotation Space Parameterization（旋转空间参数化）： We parameterize the rotation matrix with the axis-angle Representation. One major component of BnB is the branching of the search space.

This paragraph provides a detailed explanation of parameterizing the rotation matrix using the axis-angle representation and dividing the search space into eight subcubes encompassed by a bounding cube. This parameterization method and the branching operation are beneficial for conducting efficient searches in the rotation space.

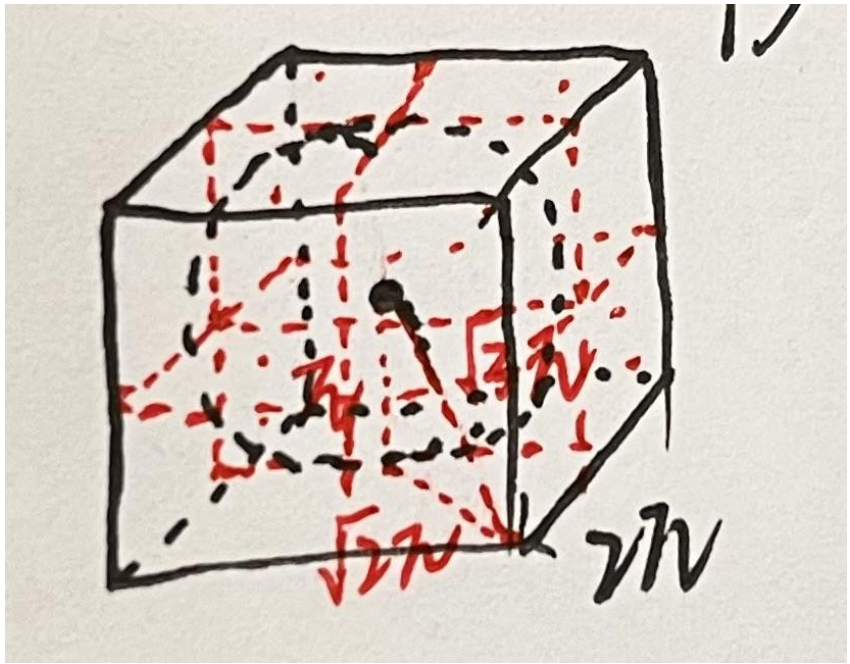

The derivations and effectiveness of the objective and upper bound functions of ROSIA

4. Previous Results: A crucial practical advantage of the axis-angle（轴角）representation is captured in the following inequality:

$$\angle(\mathbf{R_u s}, \mathbf{R_r s}) \leq \| \mathbf{u} - \mathbf{r} \| \qquad (4)$$

The significance of the inequality above is that the angular distance between two rotated vectors Rus and Rrs is upper bounded by the Euclidean distance of u and r.

The derivations and effectiveness of the objective and upper bound functions of ROSIA

the fact that the distance of any points in the cube to the center of the cube u is shorter than α_B (by construction), we state the result as follows:

$$\begin{aligned} \angle(\mathbf{R_u s}, \mathbf{R_r s}) &\leq \max_{\mathbf{r}\in\mathbb{B}} \|\mathbf{u}-\mathbf{r}\| \\ &:= \|\mathbf{u}-\mathbf{v}\| = \alpha_{\mathbb{B}} \end{aligned} \tag{5}$$

where v is one of the vertices of the cube.

The derivations and effectiveness of the objective and upper bound functions of ROSIA

(6) is the upper bound of (3)

$$\overline{Q}_{\text{ang}}(\mathbb{B}) = \sum_{i=1}^{N} \max_{1 \le j \le M} \lfloor \angle(\mathbf{R_u s}_i,\ \mathbf{c}_j) \le \alpha_\epsilon + \alpha_{\mathbb{B}} \rfloor . \qquad (6)$$

Formula (6) provides a stricter constraint on the number of matching items. It combines the angle constraint from formula (3) with the Euclidean distance constraint from formula (5).

The derivations and effectiveness of the objective and upper bound functions of ROSIA

5. Objective and Upper Bound Functions of ROSIA:

We found that the upper bound in (6) is too conservative for the Star-ID problem. Consequently, a vast majority of the search space is visited, resulting in slow convergence. Consequently, it is easy to find a match when each star in the query scene s_i is allowed to move within the domain uncertainty αB individually.（每个星星在域不确定性内移动）

Mathematically, the pattern change violates the angular distance preserving property of a rotation.

The derivations and effectiveness of the objective and upper bound functions of ROSIA

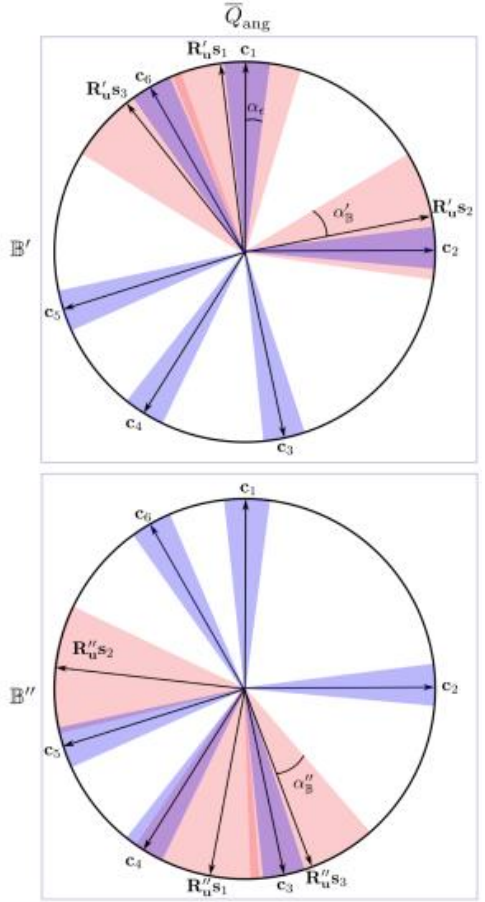

Specifically, the angular distance between c4, c5 is significantly smaller than ∠(s1,s2). Based on this key observation, we anchor each query star s_i with its neighboring stars and formulate the upper bound of ROSIA as

$$\overline{Q}_{\text{ROSIA}}(\mathbb{B}) := \sum_{i=1}^{N} \max_{1\le j\le M} \Big(\lfloor \angle(\mathbf{R_u s}_i,\ \mathbf{c}_j) \le \alpha_\epsilon + \alpha_{\mathbb{B}} \rfloor \prod_{k}^{K} \lfloor |\theta_k^{(i)} - \phi_k^{(j)}| \le 2\alpha_\epsilon \rfloor \Big) \tag{7}$$

$\theta_k^{(i)}$ - $\varphi_k^{(i)}$:represents the constraint that the absolute difference between the angles $\theta_k^{(i)}$ （第i个查询星和其邻近星的角距离）and $\varphi_k^{(i)}$

The derivations and effectiveness of the objective and upper bound functions of ROSIA

$$\{\theta_k^{(i)} \mid \theta_k^{(i)} := \angle(\mathbf{s}_i, \mathbf{s}_k), k \neq i\}_{k=1}^{N-1} \tag{8}$$

The angular distances between the ith query star and its N-1 neighboring stars are calculated and sorted in ascending order（查询星与其N-I邻星按升序排列，前两个叫三元组特征）

$$\{\phi_k^{(j)} \mid \phi_k^{(j)} := \angle(\mathbf{c}_j, \mathbf{c}_k), k \neq j\}_{k=1}^{M-1}. \tag{9}$$

the equivalent set for the jth catalog star

The derivations and effectiveness of the objective and upper bound functions of ROSIA

Since BnB requires the objective and bounding functions to have a converging property（收敛）, i.e., objective function=upper bound function when the domain collapses to a singleton (αB = 0), we incorporate the same constraint to (3) and formulate the objective function as:

$$Q_{\mathrm{ROSIA}}(\mathbf{R}) := \sum_{i=1}^{N} \max_{1 \le j \le M} \Big(\lfloor \angle(\mathbf{R}\mathbf{s}_i,\ \mathbf{c}_j) \le \alpha_\epsilon \rfloor \prod_{k}^{K} \lfloor |\theta_k^{(i)} - \phi_k^{(j)}| \le 2\alpha_\epsilon \rfloor \Big) . \qquad (10)$$

QROSIA(R) represents the value of an objective function used to evaluate the quality of the match between the query stars and the catalog stars.

The derivations and effectiveness of the objective and upper bound functions of ROSIA

The effect of the triple constraint is illustrated in Fig. 4 (right column)

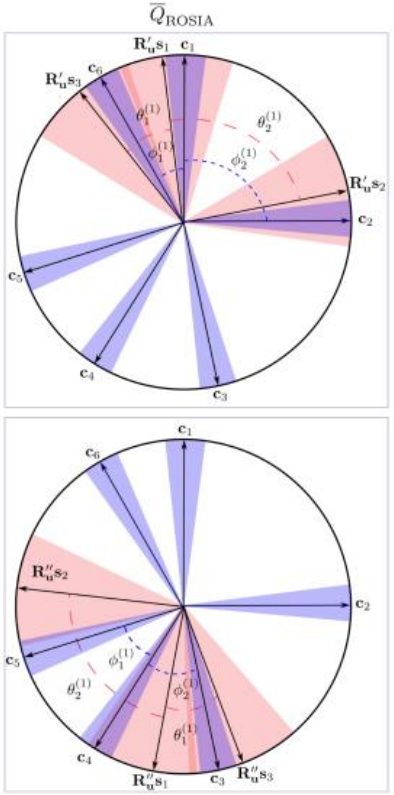

The effect of the triple constraint is illustrated in Fig. 4 (right column). The top-right figure depicts a match between $\mathbf{s}_1$ and $\mathbf{c}_1$ given $\mathbb{B}'$, where two nearest stars of $\mathbf{c}_1$, $\mathbf{c}_2$, and $\mathbf{c}_6$ form a similar pattern with the rotated query stars $\mathbf{R}'_{\mathbf{u}}\mathbf{s}_1$, $\mathbf{R}'_{\mathbf{u}}\mathbf{s}_2$, and $\mathbf{R}'_{\mathbf{u}}\mathbf{s}_3$. More specifically, $\theta_1^{(1)}$ and $\theta_2^{(1)}$ match with $\phi_1^{(1)}$ and $\phi_2^{(1)}$ (up to $2\alpha_\epsilon$), respectively. The tightness of $\overline{Q}_{\text{ROSIA}}$ is signified in the bottom right figure, where $\mathbf{R}''_{\mathbf{u}}\mathbf{s}_1$ and $\mathbf{c}_4$ are not considered as a match because $\theta_2^{(1)} >> \phi_2^{(1)}$. Trivially, the added constraining term makes $Q_{\text{ROSIA}} \leq Q_{\text{ang}}$

The derivations and effectiveness of the objective and upper bound functions of ROSIA

TABLE I
Comparing Average BnB Iterations and Runtime for (Q_{ang}, $\overline{Q}_{\text{ang}}$) Against ($Q_{\text{ROSIA}}$, $\overline{Q}_{\text{ROSIA}}$)

Objective and upper bound functions	Average iteration counts	Average runtime (s)
Q_{ang}, $\overline{Q}_{\text{ang}}$	~ 99000	~ 6.52
Q_{ROSIA}, $\overline{Q}_{\text{ROSIA}}$	~ 660	~ 0.016

As a result, the quality of each subdomain is reflected more precisely with our proposed upper bound QROSIA, which leads to much fewer search iterations.

We observed a $\sim 400\times$ speed gain compared to Qang and $\overline{\text{Qang}}$.

ROSIA

Algorithm 1: ROSIA : Rotation-Search-Based Star-ID Algorithm.

Require: Scene stars $\{\mathbf{s}_i, v_s^{(i)}\}_{i=1}^{N}$, onboard catalog $\{\mathbf{c}_j, v_c^{(j)}, \phi_1^{(j)}, \phi_2^{(j)}\}_{j=1}^{M}$, angular uncertainty α_ϵ, and magnitude uncertainty ϵ_v.

1: Extracts triplet features $\{\theta_1^{(i)}, \theta_2^{(i)}\}_{i=1}^{N}$ from the input scene stars.
2: Extracts N subcatalogs $\{\mathbf{C}^{(i)}\}_{i=1}^{N}$.
3: Stereographically projects and indexes subcatalogs into N circular R-trees.
4: Initializes $q \leftarrow$ empty priority queue, $\mathbb{B} \leftarrow$ cube of side 2π, $Q^* \leftarrow 0$, $\mathbf{R}^* \leftarrow \emptyset$.
5: Inserts $\mathbb{B}$ with priority $\overline{Q}_{\text{ROSIA}}(\mathbb{B})$ into q.
6: **while** q is not empty **do**
7: Obtain the highest priority cube $\mathbb{B}$ from q.
8: IF $\overline{Q}_{\text{ROSIA}}(\mathbb{B}) = Q^*$, terminate.
9: $\mathbf{R_u} \leftarrow$ center rotation of $\mathbb{B}$.
10: IF $Q_{\text{ROSIA}}(\mathbf{R_u}) > Q^*$, $\mathbf{R}^* \leftarrow \mathbf{R_u}$, $Q^* \leftarrow Q_{\text{ROSIA}}(\mathbf{R_u})$.
11: Subdivides $\mathbb{B}$ into 8 cubes $\{\mathbb{B}_d\}_{d=1}^{8}$.
12: For each $\mathbb{B}_d$, IF $\overline{Q}_{\text{ROSIA}}(\mathbb{B}_d) > Q^*$, insert $\mathbb{B}_d$ into q with priority $\overline{Q}_{\text{ROSIA}}(\mathbb{B}_d)$.
13: **end while**
14: **return** $\mathbf{M}^*$ and $\mathbf{R}^*$.

算法步骤：

1. 从输入的场景星体中提取三元组特征{$\theta_1^{(i)}$，$\theta_2^{(i)}$}，对每颗场景星体i都提取相邻角距离的特征。
2. 提取N个子目录{$C^{(i)}$}，将航天目录分成N个子目录，每个子目录包含了一部分目标星体。
3. 对子目录进行立体投影和索引，将每个子目录进行立体投影并构建循环R树索引结构。
4. 初始化优先级队列q、立方体B（边长为2π）、最大得分Q*和最佳匹配结果R*。*
5. 将立方体B以QROSIA(B)的优先级插入到优先级队列q中。
6. 当优先级队列q不为空时，执行以下循环：
   - 从队列q中获取优先级最高的立方体B。
   - 如果QROSIA(B)等于Q*，则终止算法。
   - 计算立方体B的中心旋转Ru。
   - 如果QROSIA(Ru)大于Q*，则更新最佳匹配结果R*和最大得分Q*。*
   - 将立方体B分成8个子立方体{Bd}，并对每个子立方体执行以下操作：
     - 如果QROSIA(Bd)大于Q*，则将Bd以QROSIA(Bd)的优先级插入到优先级队列q中。
7. 返回最佳匹配结果M*和最佳旋转结果R*。*

ROSIA

Strategy 1—Extraction of Subcatalogs（提取子目录）：

In detail, for each query scene, ROSIA first computes and ascendingly sorts all $\binom{2}{N}$ angular distances from the body-vectors$\{s_i\}_{i=1}^{N}$（查询星向量）.Then, the first two angular distances of each query star$\{\theta_1^{(i)}, \theta_2^{(i)}\}$ (the triplet feature henceforth) are extracted. The same process is also applied to the catalog stars (extraction of $\{\phi_1^{(j)}, \phi_2^{(j)}\}$) during the onboard catalog construction.

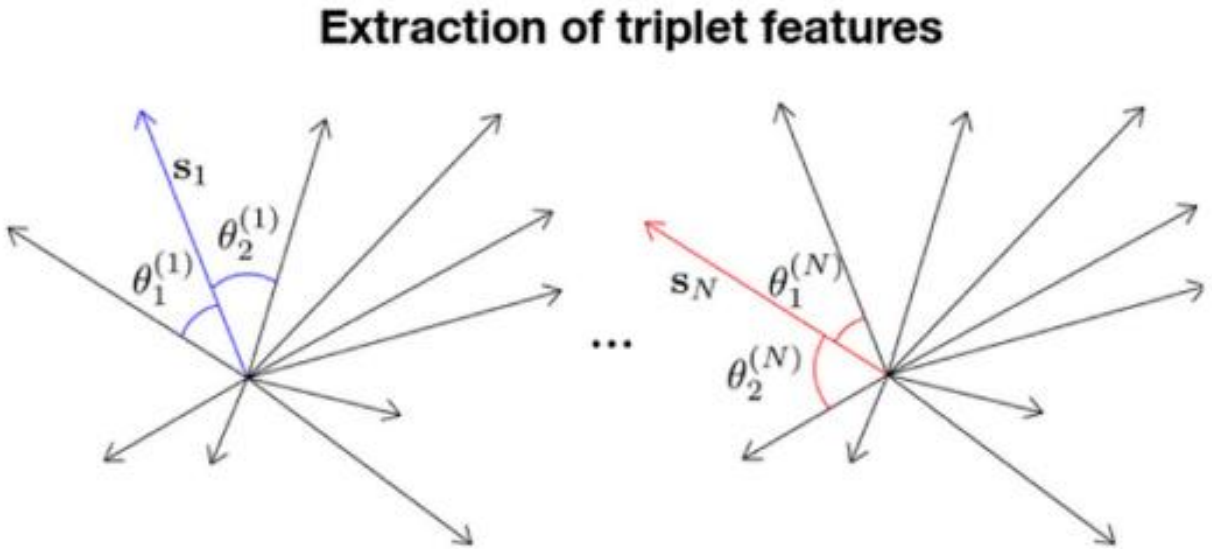

ROSIA

Then, for each query star s_i, its corresponding subcatalog is defined as:

$$\mathbf{C}_i := \{(\mathbf{c}_j, \{\phi_k^{(j)}\}_{k=1}^2, v_c{}^{(j)}) \mid |\phi_k^{(j)} - \theta_k^{(i)}| \leq 2\alpha_\epsilon \text{ and } |v_c{}^{(j)} - v_s{}^{(i)}| \leq \epsilon_v,\ j = 1 \ldots M\} \quad (11)$$

C_i: Represents the subdirectory corresponding to the query star s_i, which is a set.
c_j : Represents a star in the catalog, i.e., a catalog star.
$v_c^{(j)}$: Represents the visual magnitude of the catalog star c_j , indicating the brightness information of the catalog star.（视星，表示星表星的亮度信息）
$v_s^{(i)}$: Represents the visual magnitude of the query star s_i , indicating the brightness information of the query star.

ROSIA

Functions Q_{ROSIA} and $\bar{Q}_{ROSIA}$ given N subcatalogs $\{C_i\}_{i=1}^{N}$ can be expressed as:

$$Q_{\mathrm{ROSIA\_sub}}(\mathbf{R}) := \sum_{i=1}^{N} \max_{1 \le j \le |C_i|} \left(\lfloor \angle(\mathbf{R}\mathbf{s}_i,\ \mathbf{c}_j) \le \alpha_\epsilon \rfloor \right) \quad (12)$$

and

$$\bar{Q}_{\mathrm{ROSIA\_sub}}(\mathbb{B}) := \sum_{i=1}^{N} \max_{1 \le j \le |C_i|} \left(\lfloor \angle(\mathbf{R}_\mathbf{u}\mathbf{s}_i,\ \mathbf{c}_j) \le \alpha_\epsilon + \alpha_{\mathbb{B}} \rfloor \right) \quad (13)$$

ROSIA

Strategy 2—R-Tree Search :（立体投影和r-tree搜索）

We elaborate two key ingredients that are needed to cast the O(N Msub) catalog star query into a O(N log Msub) tree search problem here: 1) stereographic projection and 2) the R-tree indexation scheme.

Stereographic Projection to Avoid Dimension Redundancy:

We highlight that evaluating Q_{ROSIA_sub} and $\bar{Q}_{ROSIA\_sub}$ in the 3-D vector space is inefficient. we leverage stereographic projection to map spherical patches onto a 2-D plane, which in turn reduces the dimensionality of Q_{ROSIA_sub} and $\bar{Q}_{ROSIA\_sub}$ from three to two.

ROSIA

Spherical Patches（球面片）: Formally, a spherical patch defined by a 3-D unit vector x and an angular uncertainty α can be expressed as

$$S_\alpha(\mathbf{x}) = \{\mathbf{y} \mid \angle(\mathbf{y}, \mathbf{x}) \leq \alpha,\ \|\mathbf{y}\| = 1, \|\mathbf{x}\| = 1\}\ . \qquad (14)$$

There are two types of spherical patches in evaluating Q_{ROSIA_sub} and $\bar{Q}_{ROSIA\_sub}$. We denote the patch defined by a catalog star c_j and its measurement angular uncertainty αι as $S_{\alpha_\epsilon}(c_j)$, and $S_{\alpha_B}(s_i)$, represents the patch defined by a query star s_i and the domain angular uncertainty of each cube α_B. Both patches are illustrated in Fig. 5.

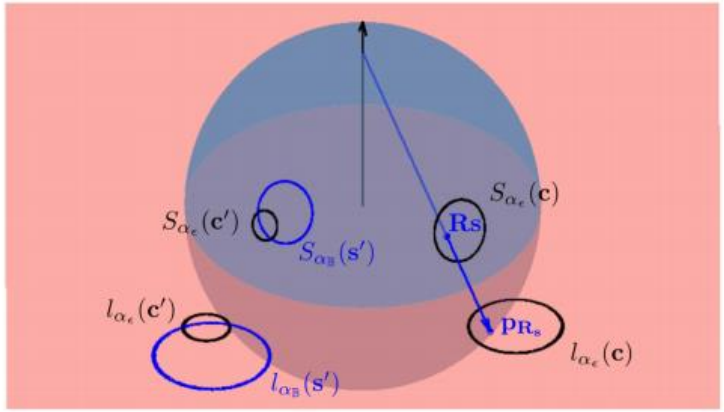

ROSIA

3-D Intersection: Geometrically, evaluating Q_{ROSIA_sub} is equivalent to determining if R_{s_i} (a 3-D point) lies within catalog patch $S_{\alpha_\epsilon}(c_j)$,(a spherical patch). Fig. 5 illustrates an example. Formally, it can be expressed as

$$\lfloor \mathbf{Rs}_i \in S_{\alpha_\epsilon}(\mathbf{c}_j) \rfloor \ . \qquad (15)$$

On the other hand, evaluating $\bar{Q}_{ROSIA\_sub}$ is equivalent to determining if a query patch $S_{\alpha_B}(s_i)$, intersects with a catalog patch $S_{\alpha_\epsilon}(c_j)$, as depicted in Fig. 5

$$\lfloor S_{\alpha_\mathbb{B}}(\mathbf{R_u s}_i) \cap S_{\alpha_\epsilon}(\mathbf{c}_j) \neq \emptyset \rfloor \ . \qquad (16)$$

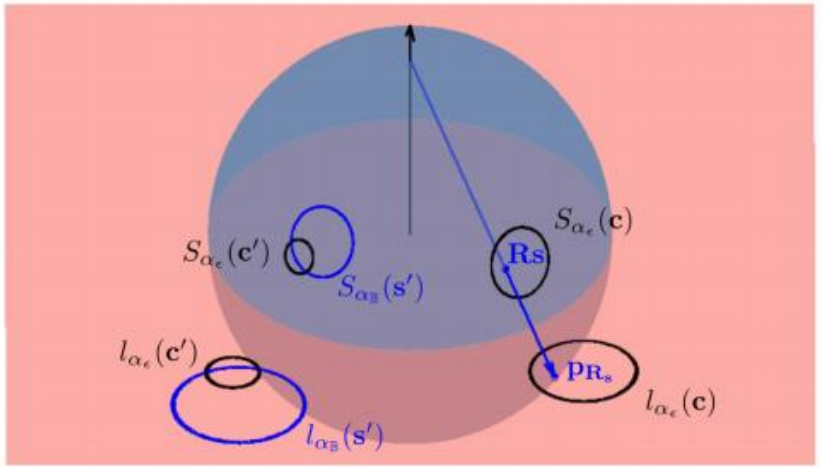

ROSIA

Stereographic Projection is Conformal, which preserves circles and circle intersections. Therefore, the circular outlines of spherical patches are projected as circles, and the intersection tasks above [(15) and (16)] can be cast into 2-D intersection tasks, which can be solved efficiently

We describe in the following, all three possible projection outcomes of spherical patches on the 2-D projection plane: interior circles, exterior circles, and half-planes. （内部圆、外部圆、半平面）

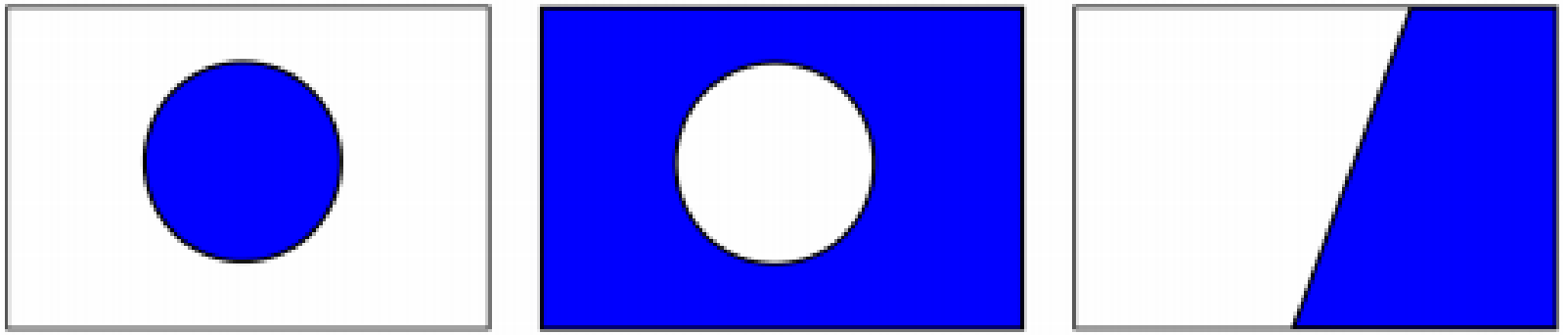

ROSIA

3-D Point to 2-D Point: We first detail the projection of a 3-D unit vector (e.g., a query star) onto the XY –plane Ω . Let [$\varphi \in [0, \pi]$, $\theta \in [0, 2\pi]$] represent the spherical coordinates of a point on the unit sphere, its stereographic projection onto Ω with N = [0, 0, 1] as the projection point can be expressed as

$$\mathbf{p} = \cot\left(\frac{\varphi}{2}\right)\begin{bmatrix}\sin(\theta)\\ \cos(\theta)\end{bmatrix}. \qquad (17)$$

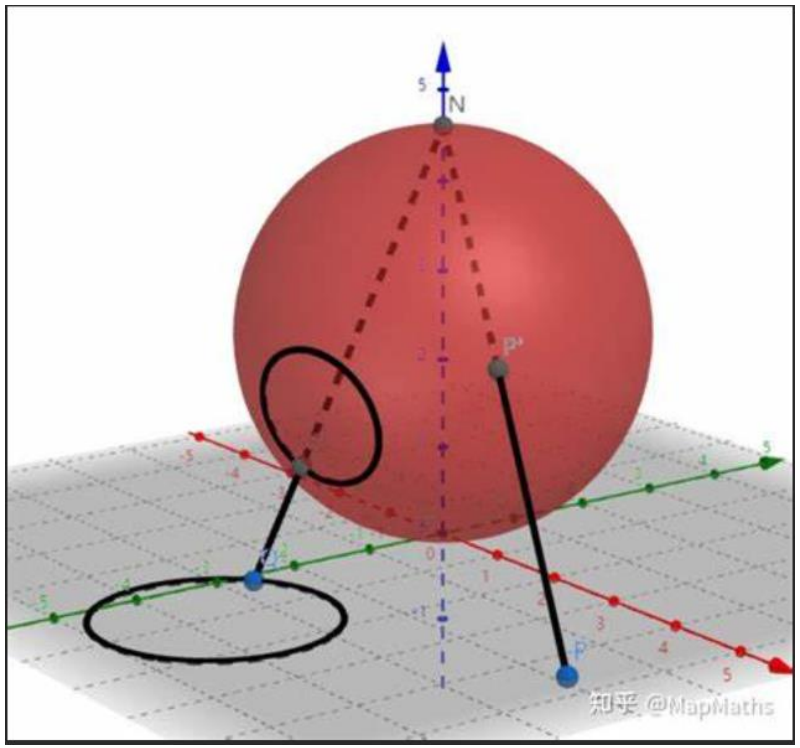

ROSIA

Spherical Patch to Interior Circle Patch: When the projection point is not part of the spherical patch, the surface is projected to the interior of a circle patch, as visualized in Fig. 6 (left). Consistent with the notation above, let [φ, θ] be the star coordinates and α be its angular uncertainty; the 2-D center point of the projected circle on χ is defined as（投影的二维中心点）

$$\mathbf{p}_c = \frac{\cot(\frac{\varphi_h}{2}) + \cot(\frac{\varphi_l}{2})}{2} \begin{bmatrix} \sin(\theta) \\ \cos(\theta) \end{bmatrix} \qquad (18)$$

where φ_h:= φ + α and φ_l := φ − α are the upper and lower bounds of the inclination angles(倾角） Meanwhile, the radius of the circle is

$$r_c = \frac{|\cot(\frac{\varphi_h}{2}) - \cot(\frac{\varphi_l}{2})|}{2} . \qquad (19)$$

ROSIA

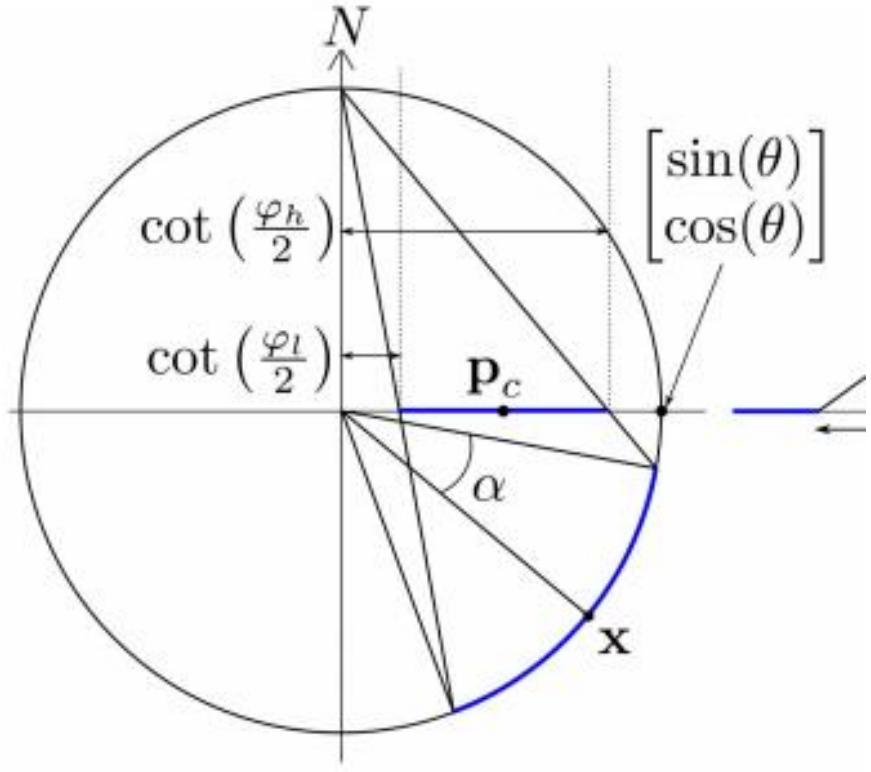

$$\mathbf{p}_c = \frac{\cot(\frac{\varphi_h}{2}) + \cot(\frac{\varphi_l}{2})}{2} \begin{bmatrix}\sin(\theta)\\ \cos(\theta)\end{bmatrix} \tag{18}$$

$$r_c = \frac{|\cot(\frac{\varphi_h}{2}) - \cot(\frac{\varphi_l}{2})|}{2} . \tag{19}$$

ROSIA

Spherical Patch to Exterior Circle Patch: When the projection point is contained within the spherical patch, the surface is projected to the exterior of a circle patch, as visualized in Fig. 6 (middle). The circle is also defined by (18) and (19), as we can see in Fig. 7 (middle).

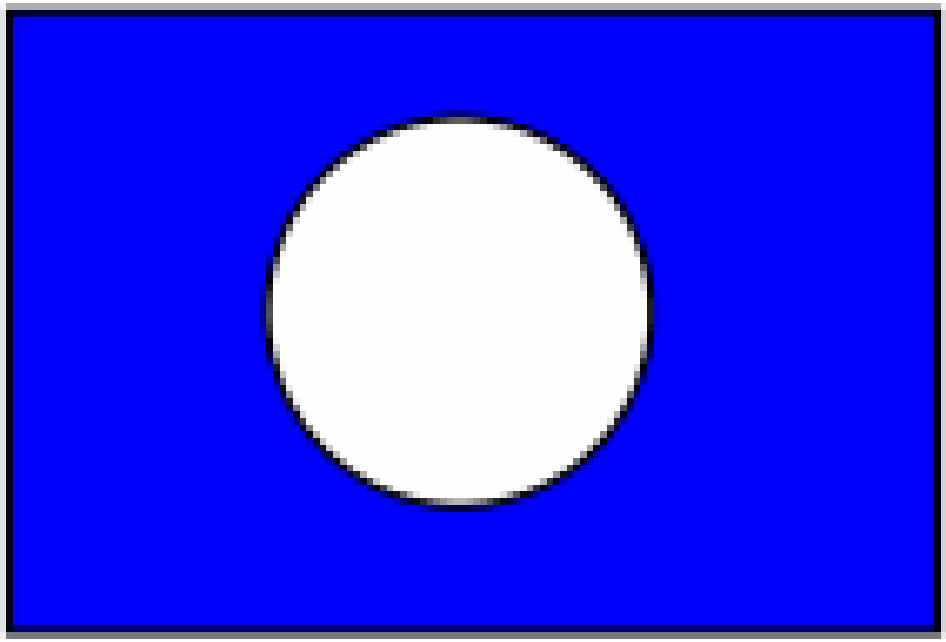

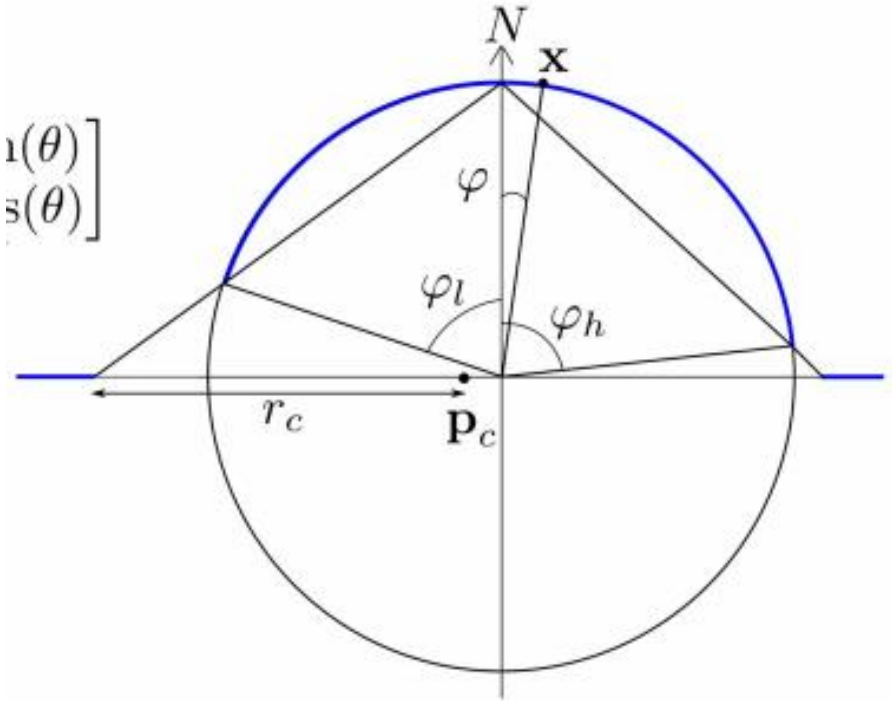

ROSIA

Spherical Patch to Half-Plane: When the projection point touches the edge of the spherical patch, i.e., φl = 0, the surface is projected to a half-plane [Fig. 6 (right)] since the projection of the projection point is at infinity [see (17)].

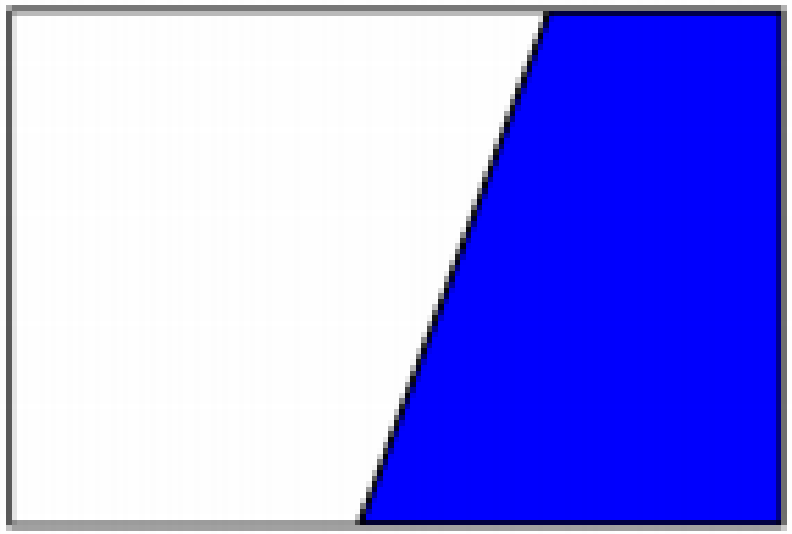

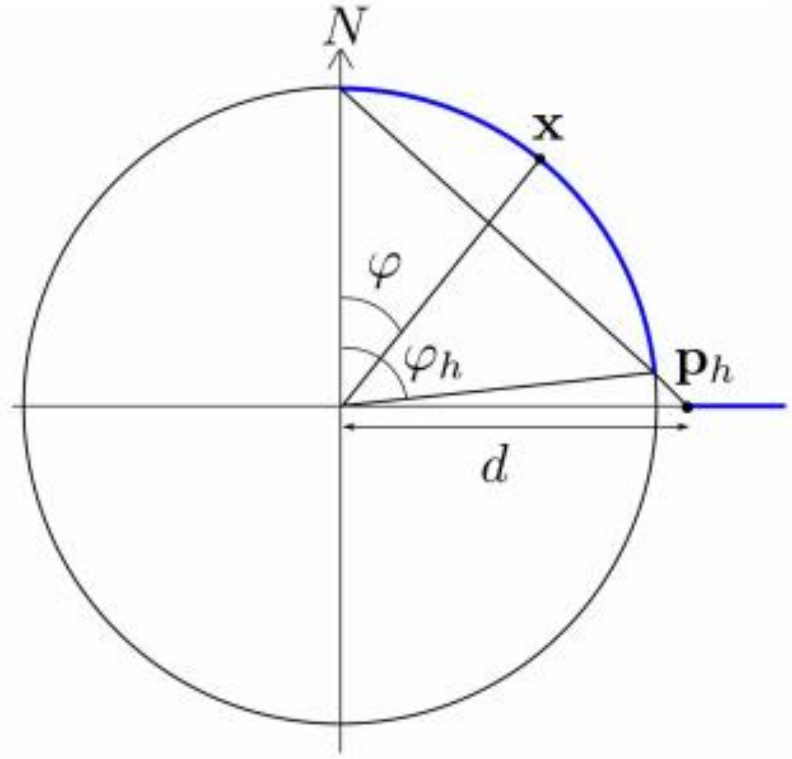

ROSIA

The half-plane is defined as

$$\begin{aligned} \hat{\mathbf{p}}_h^{\mathsf{T}}\mathbf{p} - d \geq 0 \quad \text{if} \quad \varphi_h < \pi \\ \hat{\mathbf{p}}_h^{\mathsf{T}}\mathbf{p} - d < 0 \quad \text{if} \quad \varphi_h \geq \pi \end{aligned} \tag{20}$$

where p is any arbitrary point on Ω ,$\hat{p}h$ is the direction of ph, i.e., the projection of the furthest point on the patch from the north pole.

ROSIA

2-D Intersection: Owing to the intersection preservation property, evaluating an instance of Q_{ROSIA_sub} is equivalent to checking if the (projected) query star (point) lies within a catalog star patch upon projection.(计算QROSIA_sub的实例相当于检查(投影的)查询星(点)在投影时是否在一个目录星补丁内,p是任任意点，pc是圆心)

TABLE II
Possible Point-Patch Intersection Queries on Ω

Point-Patch-intersection	Query equations
point and interior circle	$\lfloor \|\mathbf{p}' - \mathbf{p}_c\| \leq r_c \rfloor$
point and exterior circle	$\lfloor \|\mathbf{p}' - \mathbf{p}_c\| \geq r_c \rfloor$
point and half-plane	$\lfloor \hat{\mathbf{p}}_h^{\mathsf{T}} \mathbf{p}' - d \geq 0 \rfloor$ if $\varphi_h < \pi$
	$\lfloor \hat{\mathbf{p}}_h^{\mathsf{T}} \mathbf{p}' - d < 0 \rfloor$ if $\varphi_h \geq \pi$

ROSIA

On the other hand, evaluating an instance of $\bar{Q}_{ROSIA\_sub}$ is equivalent to checking if the query star patch intersects with a catalog star patch（计算QROSIA_sub的实例等价于检查查询星形补丁是否与目录星形补丁相交）

TABLE III
Possible Patch-Patch Intersection Queries on Ω

Patch-Patch-intersection	Query equations
interior circle and interior circle	$\lfloor \|\mathbf{p}'_c - \mathbf{p}_c\| \leq r'_c + r_c \rfloor$
interior circle and exterior circle	$\lfloor \|\mathbf{p}'_c - \mathbf{p}_c\| \geq r'_c + r_c \rfloor$
interior circle and half-plane	$\lfloor \hat{\mathbf{p}}_h^{\intercal}\mathbf{p}'_c - (d + r'_c) \geq 0 \rfloor$, if $\varphi_h < \pi$; $\lfloor \hat{\mathbf{p}}_h^{\intercal}\mathbf{p}'_c - (d + r'_c) < 0 \rfloor$, if $\varphi_h \geq \pi$

ROSIA

Circular R-Tree: Considering only the interior circles of catalog stars, evaluating Q_{ROSIA_sub} and $\bar{Q}_{ROSIA\ \_sub}$ translate to solving point-circle and patch-circle intersections, respectively. The interior circles can be structured geometrically in hierarchical order, as visualized in Fig. 3

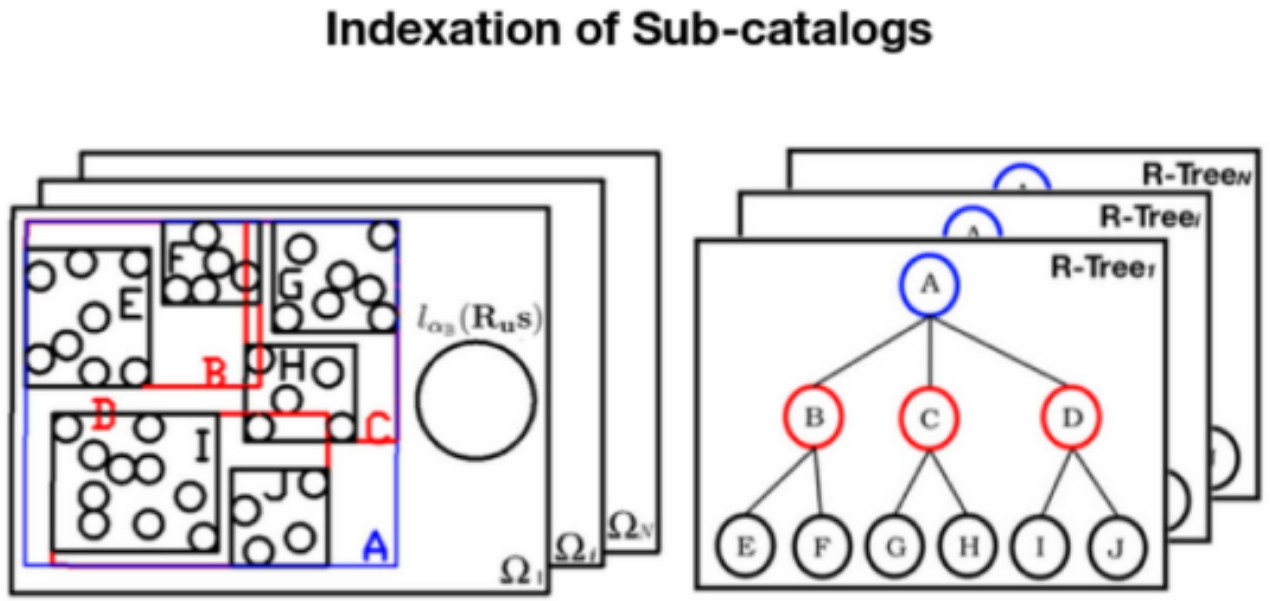

ROSIA

Matchlists: The search effort can be further improved by reducing N. Given any cube B, the intersection set between the query scene stars S : $\{s_i\}_{i=1}^{N}$ and their corresponding subcatalog $C^{(i)}$ is

$$I = \{\mathbf{s} \in \mathbf{S} \mid \exists\, \mathbf{c} \in \mathbf{C}^{(i)}, \lfloor \angle(\mathbf{R_u s},\ \mathbf{c}) \leq \alpha_\epsilon + \alpha_{\mathbb{B}} \rfloor\}\ . \quad (21)$$

The set I is coined as the matchlist of B by Breuel . By construction, the matchlist of a subcube $B' \subset$ B, is always a subset of I, i.e., $I' \subset$ I.

ROSIA

Computational Complexity: Table IV summarizes the computational cost of the main components in ROSIA. There are two main steps in the triplet feature extraction process(这段话的重点是总结了ROSIA算法中各个主要组件的计算成本)

1) the computation of $\binom{2}{N}$angular distances, and

2) sorting N angular distances for N query stars which take O(N log N) effort.

TABLE IV
Computational Complexity of ROSIA

Component	Complexity
Extraction of Triplet features	$\mathcal{O}(N^2 + N \log N)$
Extraction of Sub-catalogs	$\mathcal{O}(N \log M)$
Stereographic projection	$\mathcal{O}(N M_{\text{sub}})$
Circular R-tree building	$\mathcal{O}(N M_{\text{sub}})$
$Q_{\text{ROSIA\_sub}}$ evaluation	$\mathcal{O}(N_{\text{avg}} \log M_{\text{sub}})$
$\overline{Q}_{\text{ROSIA\_sub}}$ evaluation	$\mathcal{O}(N_{\text{avg}} \log M_{\text{sub}})$

EXPERIMENTS

We evaluated ROSIA with both simulated and real data in this section. We first conducted controlled experiments using simulated data to analyze the performance of ROSIA against different noise sources thoroughly. In addition, we compared ROSIA with the state-of-the-art MPA [18]. To enhance the performance of MPA, we incorporated the visual magnitude information, as described in [40]. We report the identification rate, the rate of no-result, and the false positive rate for both algorithms. In addition, we also report the average runtime and memory consumption of ROSIA to showcase its feasibility.

Simulated Data Experiments

- We generated our input data with the scripts released by the organizers of the European Space Agency (ESA) Star Trackers: First contact competition.The HIPPARCOS catalog is utilized in the data generation.
- ROSIA and MPA share two hyperparameters: 1) the angular distance deviation threshold α_ϵ and 2) the magnitude deviation threshold6 ϵ_v.
- The ROSIA and MPA algorithms were evaluated under three sets of common hyperparameters, namely S1, S2, and S3.

S1 = {α_ϵ=0.0205°, ϵ_v =0.45},S2 = {α_ϵ= 0.0275°, ϵ_v =0.6}, S3 = {α_ϵ =0.0275°, ϵ_v =1.2}

Simulated Data Experiments

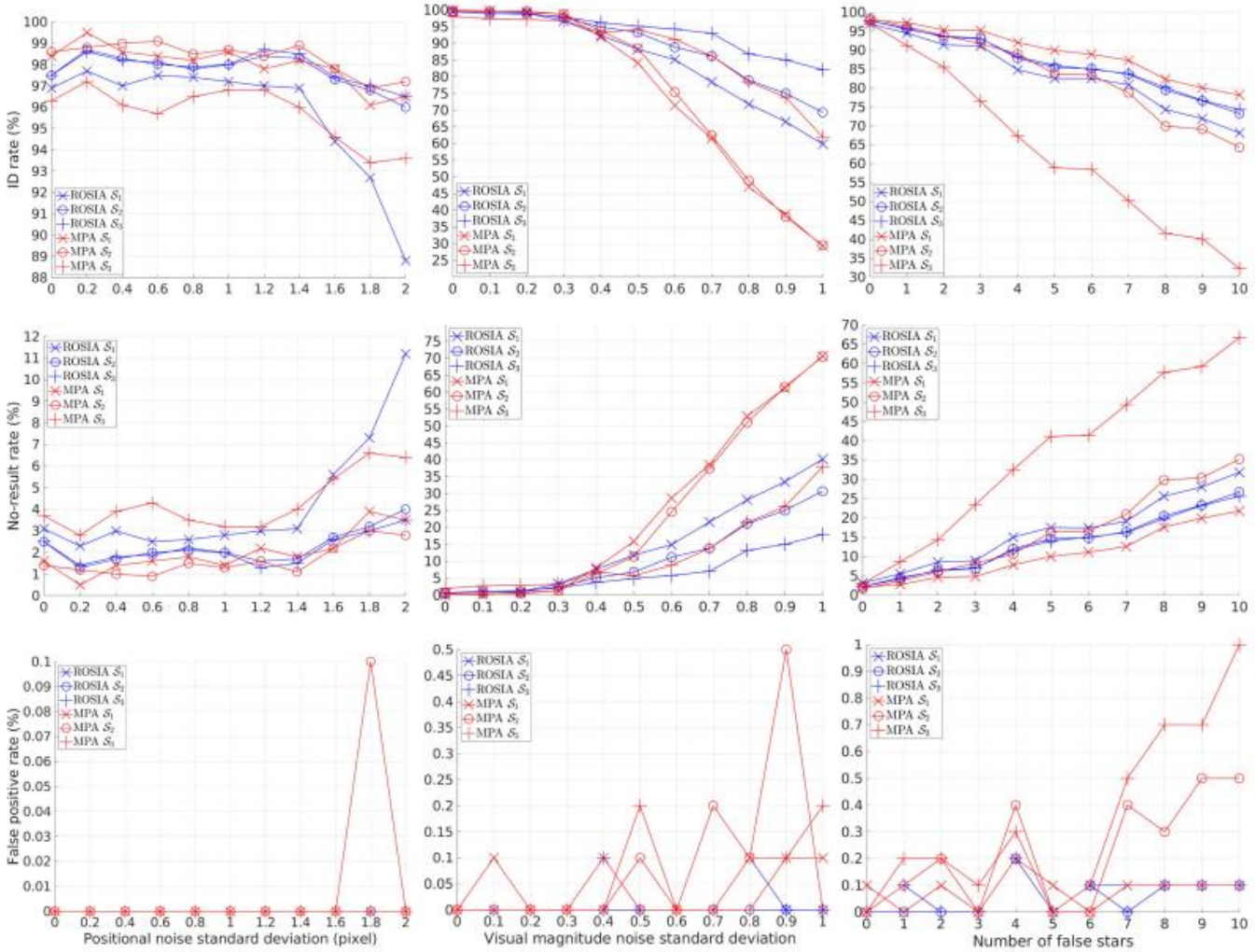

Performance of ROSIA (in blue) and MPA (in red) against different sources of noise. Top row: ID rate. Middle row: No-result rate. Bottom row: False positive rate. S1, S2, and S3 denote three hyperparameters configurations. S1(–x–) and S2(–◦–) are set at 1.5σ and 2σ of the standard pixel and visual magnitude noise, i.e., 1 pixel and 0.3 magnitudes. S3(– + –) covers the maximum (pixel and magnitude) noise SDs.

Simulated Data Experiments

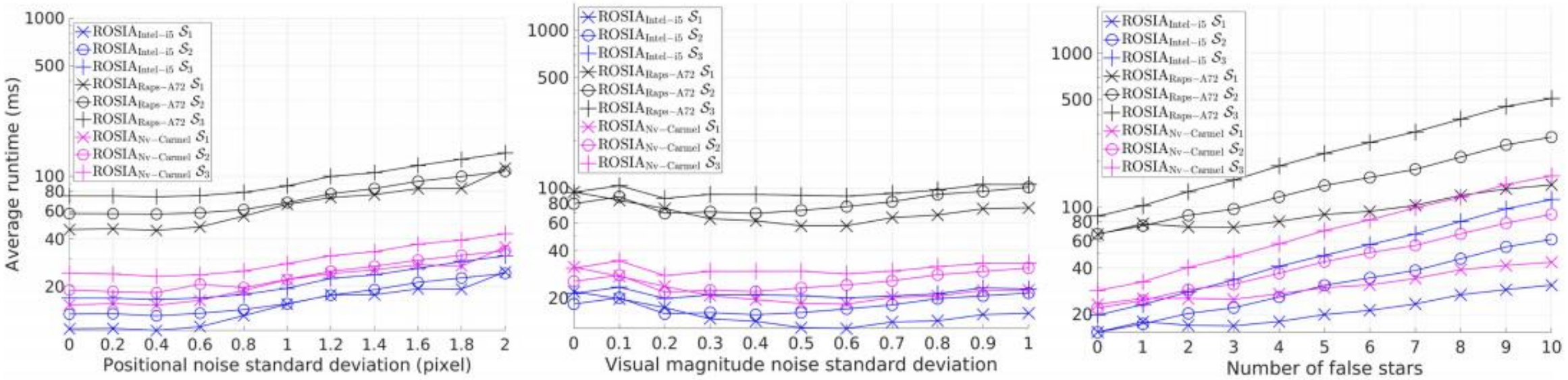

Average runtime of ROSIA. Note the log scale of the y-axis. Consistent notations with Fig. 8. The subscripts “Intel-i5,” “Raps-A72,” and “Nv-Carmel” differentiates the processor types used in our experiments.

Simulated Data Experiments

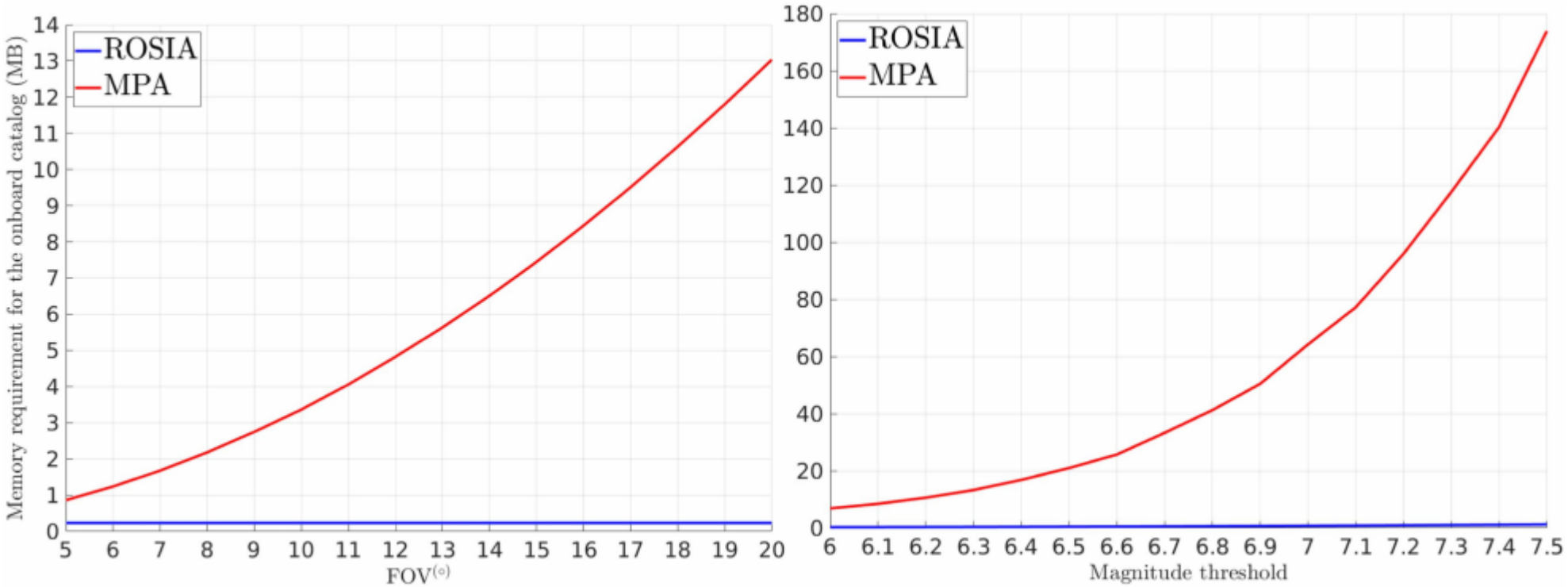

Memory requirement of ROSIA and MPA for the onboard catalog against different camera FOVs and visual magnitude thresholds.

Real Data Experiments

Details of the Real Star Images and Runtime Results

Constellation	input count	Angle deviation(○)	Runtime (ms)		
			i5	A72	Carmel
Coma Berenices	19	0.01	6.6	50.6	18.3
Carina	23	0.008	11.6	101.8	37.1
Ursa Major	18	0.06	15.5	124.9	44.2
Centaurus	30	0.04	57.3	826	279

Real Data Experiments

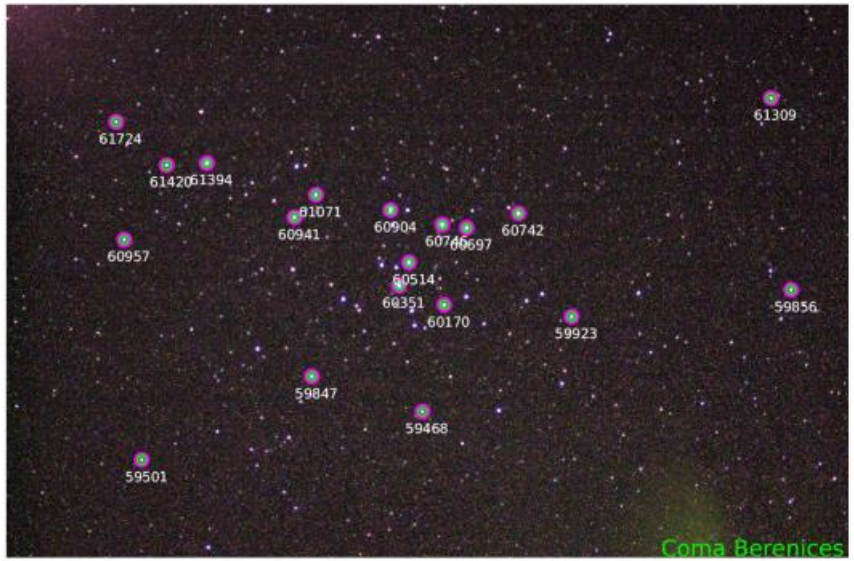

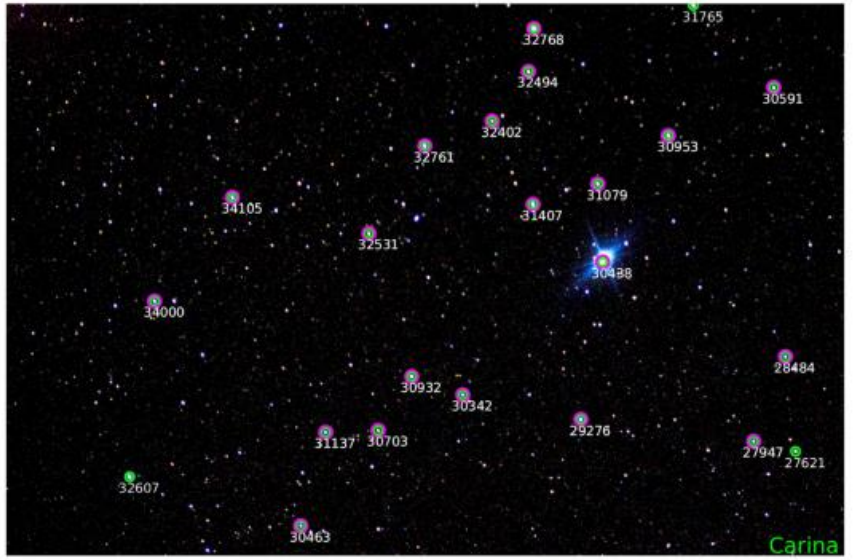

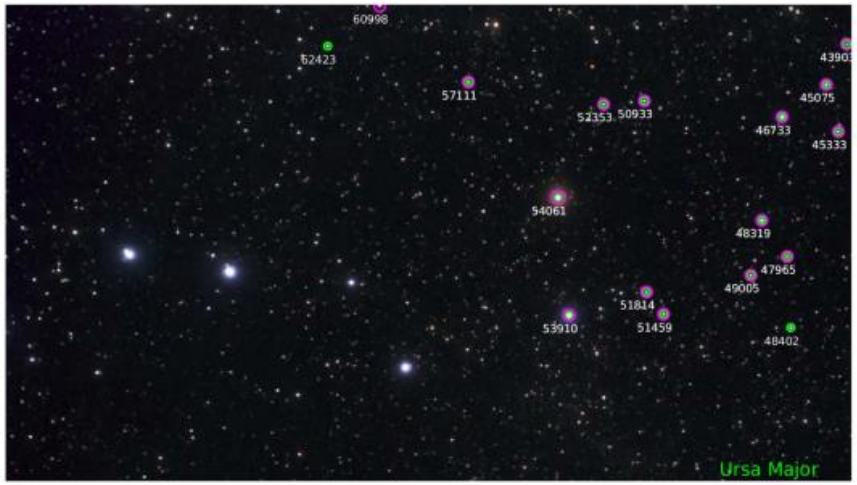

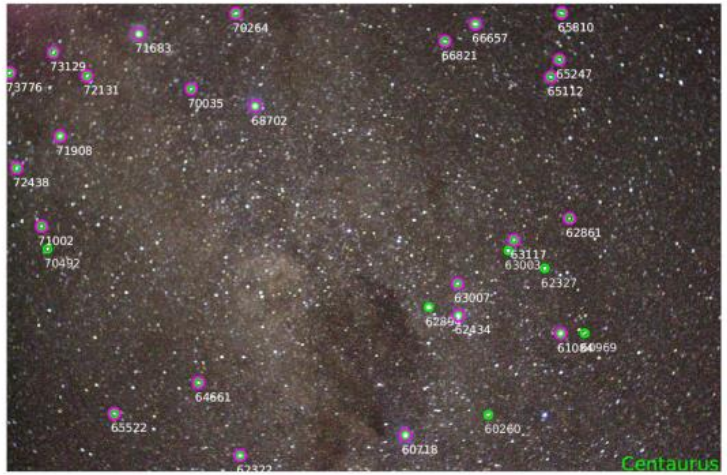

Thank You!

Avenida da Universidade, Taipa, Macau, China
Tel : (853) 8822 8833 Fax : (853) 8822 8822
Email : info@um.edu.mo Website : www.um.edu.mo